Adaptive self-calibrating image rejection receiver.

Ediz Cetin
Izzet Kale
Richard Morling

Cavendish School of Computer Science

ADAPTIVE SELF-CALIBRATING IMAGE REJECTION RECEIVER

Ediz Çetin, İzzet Kale and Richard C. S. Morling
Department of Electronic Systems, Applied DSP and VLSI Research Group,
University of Westminster
London, United Kingdom

Abstract— **An adaptive self-calibrating image rejection receiver is described, containing a modified Weaver image rejection mixer and a *Digital Image Rejection Processor* (DIRP). The blind source-separation-based DIRP eliminates the I/Q errors improving the *Image Rejection Ratio* (IRR) without the need for trimming or use of power-hungry discrete components. Hardware complexity is minimal, requiring only two complex coefficients; hence it can be easily integrated into the signal processing path of any receiver. Simulation results show that the proposed approach achieves 75-97 dB of IRR.**

Keywords- Image-rejection-receiver, Adaptive I/Q-correction, Phase and gain mismatch,Unsupervised/Blind signal processing.

I. INTRODUCTION

Image rejection receivers utilize in-phase and quadrature (I/Q) signal processing in processing of bandpass signals. However, analog implementations of I/Q signal processing is vulnerable to phase and gain mismatches between the I and Q branches of the receiver. This results in imperfect image rejection, which is not sufficient for communications applications leading to severe performance degradation. Therefore, digital techniques which will enhance this image rejection and alleviate the I and Q channel mismatches play an important role in simplifying the analog front-ends in future high performance highly-integrated single-chip wireless receivers.

Conventional image rejection architectures are implemented by analog circuit techniques [1]–[4]. However, hybrid and digital solutions have also been reported in the literature trying to improve IRR [5] - [7].

In this paper we propose digital self-calibrating image rejection receiver architecture to overcome the performance degradation due to analog front-end nonlinearities. The proposed technique uses unsupervised/blind digital signal processing techniques to estimate nonlinearities and compensate for them in real-time during the normal operation of the receiver. The receiver can adapt its configuration to the environment, a major factor for maintaining performance under almost all circumstances. What is more, the algorithm can be easily integrated into the standard digital signal processing path for any receiver with a minimal hardware overhead.

The paper is organized as follows: Section II defines the architecture of the adaptive image rejection receiver. Section III describes the performance analysis and the simulation results, while concluding remarks are given in Section IV.

II. ADAPTIVE IMAGE REJECTION RECEIVER ARCHITECTURE

This section describes the self-calibrating adaptive image rejection receiver architecture, block diagram of which is shown in Fig. 1. In this architecture, a *Radio Frequency* (RF) signal is received by an antenna and passed through an RF front-end to produce a bandpass signal. This signal is then digitised and sent to an image-rejection receiver to suppress the image signal increasing the image rejection that can be achieved.

The self-calibrating adaptive image rejection receiver can be divided into two parts. First part is the modified Weaver image rejection mixer, and the second part is the *Digital Image Rejection Processor* (DIRP). The modified Weaver image rejection mixer generates two complex digital output signals, $r_1(k)$ and $r_2(k)$, where the signal $r_1(k)$ emphasizes the desired signal and $r_2(k)$ emphasizes the image signal. The DIRP utilizes both signals $r_1(k)$ and $r_2(k)$ to achieve increased degree of image rejection.

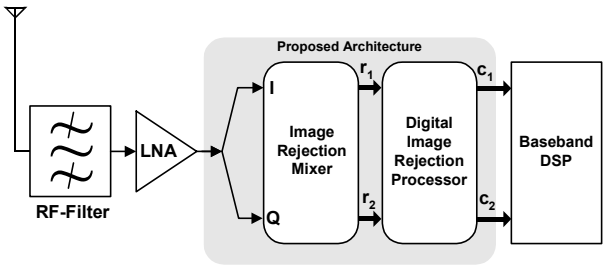

Figure 1. Image rejection receiver system.

In the following two subsections we first describe the image rejection mixer. Then we introduce the DIRP.

A. Image Rejection Mixer

The block diagram of the modified Weaver image rejection mixer is shown in Fig. 2. The incoming signal, $s(t)$, consists of the wanted signal $u(t)$ at f_{RF} and unwanted image signal $i(t)$ at f_{IMG} where $f_{IMG} = f_{RF} - 2f_{IF}$. Hence, the incoming signal $s(t)$ can be expressed as:

$$s(t) = \Re\left\{ u(t)e^{j2\pi f_{RF}t} \right\} + \Re\left\{ i(t)e^{j2\pi f_{IMG}t} \right\} \quad (1)$$

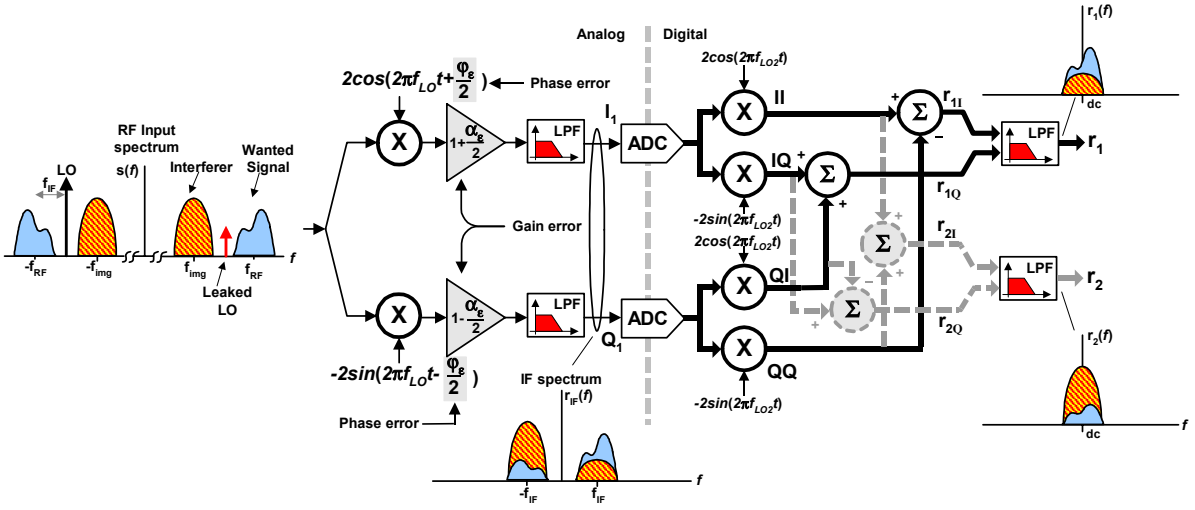

Figure 2. Image Rejection Mixer.

where $u(t)$ and $i(t)$ are the complex envelopes of the wanted and image signals respectively. To simplify the analysis, whole phase and gain imbalances between the I and Q channels are modelled as an unbalanced quadrature downconverter [8]. The erroneous complex LO signal, $x_{LO}(t)= I_{LO}+jQ_{LO}$, is given as:

$$x_{LO}(t) = e^{j2\pi f_{LO}t}(g_1 e^{j\frac{\varphi_\varepsilon}{2}} - g_2 e^{-j\frac{\varphi_\varepsilon}{2}}) + e^{-j2\pi f_{LO}t}(g_1 e^{-j\frac{\varphi_\varepsilon}{2}} + g_2 e^{j\frac{\varphi_\varepsilon}{2}}) \quad (2)$$

where $g_1=(1+0.5\alpha_\varepsilon)$, $g_2=(1-0.5\alpha_\varepsilon)$ and φ_ε is the phase and α_ε is the gain mismatch between the I and Q channels. As shown in Fig. 2, the received signal $s(t)$ is quadrature mixed with the non-ideal LO signal, x_{LO}, and low-pass filtered resulting in an IF signal $r_{IF}(t)= I_1+jQ_1$, which can be expressed as:

$$r_{IF}(t) = \tfrac{1}{2}[u(t)(g_1 e^{-j\frac{\varphi_\varepsilon}{2}} + g_2 e^{j\frac{\varphi_\varepsilon}{2}})e^{j2\pi f_{IF}t} + u^*(t)(g_1 e^{j\frac{\varphi_\varepsilon}{2}} - g_2 e^{-j\frac{\varphi_\varepsilon}{2}})e^{-j2\pi f_{IF}t}] + \quad (3)$$
$$\tfrac{1}{2}[i^*(t)(g_1 e^{j\frac{\varphi_\varepsilon}{2}} - g_2 e^{-j\frac{\varphi_\varepsilon}{2}})e^{j2\pi f_{IF}t} + i(t)(g_1 e^{-j\frac{\varphi_\varepsilon}{2}} + g_2 e^{j\frac{\varphi_\varepsilon}{2}})e^{-j2\pi f_{IF}t}]$$

where the desired signal $u(t)$ is corrupted by the image $i^*(t)$ leaked in-band due to analog mismatches. There is also a leakage from the desired signal into the image channel. A frequency domain illustration, $r_{IF}(f)$, of this is given Fig. 2. In a fully balanced system, however, the wanted signal and the interferer are downconverted to opposite frequencies $+f_{IF}$ and $-f_{IF}$. Signals I_1 and Q_1 are then converted into the digital domain. Following this, another mixer stage takes care of the final downconversion from IF to baseband. As this conversion stage takes place in the digital domain, the I and Q channels are matched hence, ideal mixing is assumed leading to the following set of four signals:

$$\begin{aligned} II &= g_1[u(t)e^{-j\frac{\varphi_\varepsilon}{2}} + u^*(t)e^{j\frac{\varphi_\varepsilon}{2}} + i(t)e^{-j\frac{\varphi_\varepsilon}{2}} + i^*(t)e^{j\frac{\varphi_\varepsilon}{2}}] \\ IQ &= jg_1[-u(t)e^{-j\frac{\varphi_\varepsilon}{2}} + u^*(t)e^{j\frac{\varphi_\varepsilon}{2}} + i(t)e^{-j\frac{\varphi_\varepsilon}{2}} - i^*(t)e^{j\frac{\varphi_\varepsilon}{2}}] \\ QI &= jg_2[-u(t)e^{j\frac{\varphi_\varepsilon}{2}} + u^*(t)e^{-j\frac{\varphi_\varepsilon}{2}} - i(t)e^{j\frac{\varphi_\varepsilon}{2}} + i^*(t)e^{-j\frac{\varphi_\varepsilon}{2}}] \\ QQ &= -g_2[u(t)e^{j\frac{\varphi_\varepsilon}{2}} + u^*(t)e^{-j\frac{\varphi_\varepsilon}{2}} - i(t)e^{j\frac{\varphi_\varepsilon}{2}} - i^*(t)e^{-j\frac{\varphi_\varepsilon}{2}}] \end{aligned} \quad (4)$$

The I and Q signals of the desired channel corrupted by the image signal due to the phase and gain errors can be expressed as:

$$\begin{aligned} r_{1I} &= II - QQ \\ &= u(t)(g_1 e^{-j\frac{\varphi_\varepsilon}{2}} + g_2 e^{j\frac{\varphi_\varepsilon}{2}}) + u^*(t)(g_1 e^{j\frac{\varphi_\varepsilon}{2}} + g_2 e^{-j\frac{\varphi_\varepsilon}{2}}) + \\ &\quad i(t)(g_1 e^{-j\frac{\varphi_\varepsilon}{2}} - g_2 e^{j\frac{\varphi_\varepsilon}{2}}) + i^*(t)(g_1 e^{j\frac{\varphi_\varepsilon}{2}} - g_2 e^{-j\frac{\varphi_\varepsilon}{2}}) \\ r_{1Q} &= IQ + QI \\ &= j[-u(t)(g_1 e^{-j\frac{\varphi_\varepsilon}{2}} + g_2 e^{j\frac{\varphi_\varepsilon}{2}}) + u^*(t)(g_1 e^{j\frac{\varphi_\varepsilon}{2}} + g_2 e^{-j\frac{\varphi_\varepsilon}{2}}) + \\ &\quad i(t)(g_1 e^{-j\frac{\varphi_\varepsilon}{2}} - g_2 e^{j\frac{\varphi_\varepsilon}{2}}) - i^*(t)(g_1 e^{j\frac{\varphi_\varepsilon}{2}} - g_2 e^{-j\frac{\varphi_\varepsilon}{2}})] \end{aligned} \quad (5)$$

Combining them as $r_{1I}+jr_{1Q}$ yields:

$$r_1(k) = u(t)\overbrace{(g_1 e^{-j\frac{\varphi_\varepsilon}{2}} + g_2 e^{j\frac{\varphi_\varepsilon}{2}})}^{h_1} + i^*(t)(g_1 e^{j\frac{\varphi_\varepsilon}{2}} - g_2 e^{-j\frac{\varphi_\varepsilon}{2}}) \quad (6)$$

This contains the desired signal corrupted by the image signal scaled by h_1, superimposed due to the phase and gain errors. This is demonstrated in the frequency domain in the top-right corner of Fig. 2. The Weaver architecture is further extended, at the expense of 2 extra adders, to provide another channel, $r_2(k)$, which contains the image signal interfered by the desired signal due to I/Q errors (marked as ▬ ▬ on Fig. 2). The I and Q signals of $r_2(k)$ can be expressed as:

$$\begin{aligned} r_{2I} &= II + QQ \\ &= u(t)(g_1 e^{-j\frac{\varphi_\varepsilon}{2}} - g_2 e^{j\frac{\varphi_\varepsilon}{2}}) + u^*(t)(g_1 e^{j\frac{\varphi_\varepsilon}{2}} - g_2 e^{-j\frac{\varphi_\varepsilon}{2}}) + \\ &\quad i(t)(g_1 e^{-j\frac{\varphi_\varepsilon}{2}} + g_2 e^{j\frac{\varphi_\varepsilon}{2}}) + i^*(t)(g_1 e^{j\frac{\varphi_\varepsilon}{2}} + g_2 e^{-j\frac{\varphi_\varepsilon}{2}}) \\ r_{2Q} &= IQ - QI \\ &= j[-u(t)(g_1 e^{-j\frac{\varphi_\varepsilon}{2}} - g_2 e^{j\frac{\varphi_\varepsilon}{2}}) + u^*(t)(g_1 e^{j\frac{\varphi_\varepsilon}{2}} - g_2 e^{-j\frac{\varphi_\varepsilon}{2}}) + \\ &\quad i(t)(g_1 e^{-j\frac{\varphi_\varepsilon}{2}} + g_2 e^{j\frac{\varphi_\varepsilon}{2}}) - i^*(t)(g_1 e^{j\frac{\varphi_\varepsilon}{2}} + g_2 e^{-j\frac{\varphi_\varepsilon}{2}})] \end{aligned} \quad (7)$$

Combining them as $r_{2I}+jr_{2Q}$ yields:

$$r_2(k) = u(t)\overbrace{(g_1 e^{-j\frac{\varphi_\varepsilon}{2}} - g_2 e^{j\frac{\varphi_\varepsilon}{2}})}^{h_2} + i^*(t)(g_1 e^{j\frac{\varphi_\varepsilon}{2}} - g_2 e^{-j\frac{\varphi_\varepsilon}{2}})] \quad (8)$$

where the image signal is corrupted by desired signal scaled by h_2. The frequency domain representation of $r_2(k)$ is given in the bottom-right corner of Fig. 2. It can be observed from (7) and (8) that the mixing coefficients h_1 and h_2 can be expressed as:

$$h_1 = h_2 = (g_1 e^{j\frac{\varphi_\varepsilon}{2}} - g_2 e^{-j\frac{\varphi_\varepsilon}{2}}) \quad (9)$$

Hence, expanding (9) yields:

$$h_1 = h_2 = \alpha_\varepsilon \cos(0.5\varphi_\varepsilon) + j2\sin(0.5\varphi_\varepsilon) \quad (10)$$

Signals $r_1(k)$ and $r_2(k)$ form the two inputs of the DIRP. To examine the performance of the mixer, we define the *Image-Rejection Ratio* (IRR) as the ratio between the desired signal to image signal. This as a function of phase and gain errors (α_ε, φ_ε) is given in decibels as:

$$IRR(\alpha_\varepsilon, \varphi_\varepsilon) = 10\log\left(\frac{2 - 2\cos\varphi_\varepsilon + 0.5\alpha_\varepsilon^2(1+\cos\varphi_\varepsilon)}{2 + 2\cos\varphi_\varepsilon + 0.5\alpha_\varepsilon^2(1-\cos\varphi_\varepsilon)}\right) \quad (11)$$

This IRR is visually depicted in Fig. 3. In order to achieve an IRR of 60 dB, phase and gain errors must be 0.01 dB and 0.1° respectively, revealing very stringent, matching requirements. In practice, analog mismatches limit the IRR to 25 – 40 dB [7].

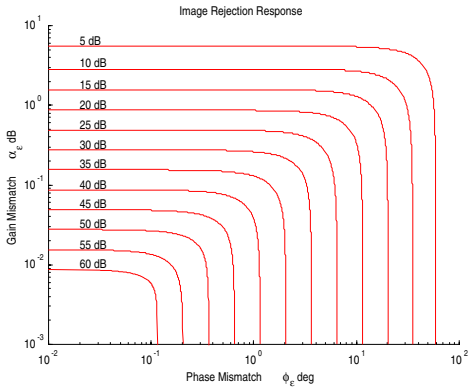

Figure 3. IRR as a function of phase and gain errors.

B. *Digital Image-Rejection-Processor (DIRP)*

To enhance the IRR performance of the modified Weaver image rejection mixer, the mismatching effects in the analog devices must be compensated digitally. In the DIRP, we compensate for the mismatches by eliminating the image signal component in the output signal $c_1(k)$. The block diagram of the feed-forward implementation of the DIRP is shown in Fig. 4. This processor contains two complex multipliers and complex LMS update hardware. For clarity, we define:

- $u(t)$ and $i(t)$ as sources.
- $r_1(k)$ and $r_2(k)$ as available observations. Expressed by (6) and (8).
- $c_1(k)$ and $c_2(k)$ as recovered sources. $c_1(k)$ is the desired channel that we are interested in.

w_1 and w_2 are both complex. The source estimates, $c_1(z)$ and $c_2(z)$, become:

$$\begin{aligned} c_1(z) &= (1 - w_1 h_2)u(z) + (h_1 - w_1)i(z) \\ c_2(z) &= (h_2 - w_2)u(z) + (1 - w_2 h_1)i(z) \end{aligned} \quad (12)$$

When the filters converge, i.e. $w_1 = h_1$ and $w_2 = h_2$ then the source estimates become:

$$\begin{aligned} c_1(z) &= (1 - h_1 h_2)u(z) \\ c_2(z) &= (1 - h_1 h_2)i(z) \end{aligned} \quad (13)$$

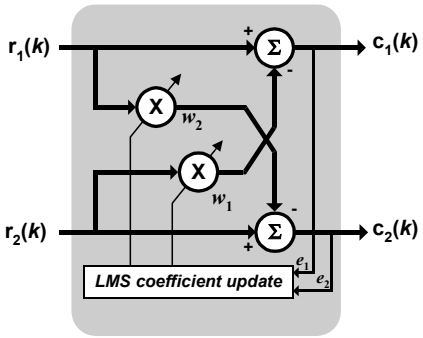

Figure 4. DIRP, feed-forward structure.

As it can be seen from (13) the sources have been separated. Also, $(1-h_1h_2) \approx 1$ and can be safely ignored. An alternative implementation for the separation structure is found by simply placing the filters in the feedback loop [8]. The Least-Mean-Squares (LMS) algorithm [9] is used to update filter coefficients. The update equations are given as:

$$\begin{aligned} w_1^{(k+1)}(m) &= w_1^{(k)}(m) + 2\mu_1 c_1(k) r_2(k-m) \qquad m = 0...L_1 \\ w_2^{(k+1)}(n) &= w_2^{(k)}(n) + 2\mu_2 c_2(k) r_1(k-n) \qquad n = 0...L_2 \end{aligned} \quad (14)$$

where, L_1 and L_2 are the filter orders. In this case both w_1 and w_2 have complex single tap coefficients.

III. Performance Analysis

A. *Simulation Setup*

The performance of the proposed structure is analysed considering QPSK, 8/32-PSK and 16/32/256-QAM signals with ideal symbol rate sampling. For all simulations, interfering signal is assumed to be 20 dB stronger than the desired one. AWGN and Multipath Rayleigh Fading channels were assumed.

The performance of the adaptive algorithm is characterized by the modelling-error [8]. This gives a global figure for the quality of the identification of the coupling coefficients h_1 and h_2 by w_1 and w_2. It is defined as the squared norm of the difference of the values between the original coefficients used in the mixture and the estimated coefficients, relative to the squared norm of the mixture coefficients. Another performance measure used is the IRR descried in (11).

B. *Tracking Capabilities*

Another performance measure is the capability of the adaptive algorithm in tracking non-stationary environments, i.e. time varying phase and gain errors. In order to show the robustness of the proposed approach we start by adapting the filters to 15° (φ_ε= 0.2618 rad) phase and 1 dB (α_ε= 0.1150) of gain error. After 6000 frames, the amplitude imbalance is changed linearly from 1 dB to 2 dB. (α_ε = 0.2292). After further 4000 frames, an abrupt change from 2 dB to 3 dB (α_ε = 0.3420) is made and the phase error is abruptly changed to 30° (φ_ε = 0.5236 rad). 4000 frames later, the phase error is changed linearly from 30° to reach 40° (φ_ε = 0.6981 rad) for the next 1000 frames. Fig. 5 depicts the tracking capability of the proposed algorithm (a) for QPSK modulation and (b) for 16-QAM modulation schemes in the presence of AWGN channel with SNR of 20 dB.

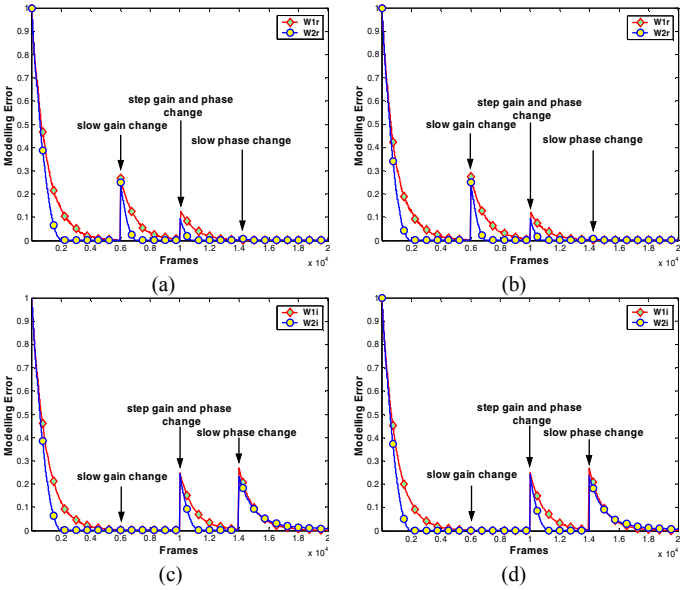

Figure 5. Tracking capabilities of the proposed algorithm, (a), (c) QPSK and (b), (d) 16-QAM case.

As can be seen from Fig. 5, a sudden change in the mixture coefficients, and phase and gain errors, does not cause the algorithm to diverge and the algorithm tracks the changes rapidly and the modelling error is zeroed. In addition, the compensator performance is not affected by time-variant phase and gain errors. This indicates that the proposed method is also capable of tracking time-varying imbalances. As can be observed from Fig. 5 (c) and (d), as expected, gain change has not affected the modelling error since w_{1i} and w_{2i} are dependent only on the phase change (cf. (10)). On the other hand, w_{1r} and w_{2r} both depend on the phase and gain errors. This can be observed from Fig. 5 (a) and (b).

C. *Multi-Path and Fading Channels*

Another performance measure is the capability of the adaptive algorithm to perform under fading and multi-path environments. The robustness of the proposed approach in a more realistic environment than the AWGN channel is demonstrated using a Rayleigh Fading channel with multipath. Fig. 6 depicts the channel profiles, received signal power over time for (a) slow fading and (b) fast fading with a multipath Rayleigh channel. Fig. 7 shows the simulation results.

As can be seen from Fig. 7, the proposed algorithm is able to work under both slow and fast fading multipath channels and the modelling error is effectively zeroed. Table I depicts the resulting tap estimates w_1 and w_2, residual gain and phase errors and the steady-state IRR for QPSK and 16-QAM modulated signals in slow and fast fading multipath environments.

Further simulation results are given in Figs. 8-10 for varying phase and gain errors respectively. As well as varying both at the same time. We can observe from Fig. 10, on average 70 dB improvement in IRR after compensation is achieved.

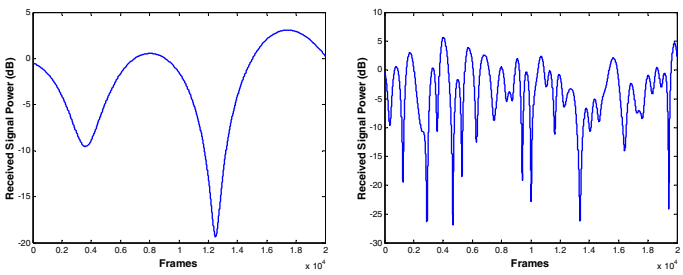

Figure 6. Channel profiles for (a) slow fading and (b) fast fading, multipath Rayleigh Channel.

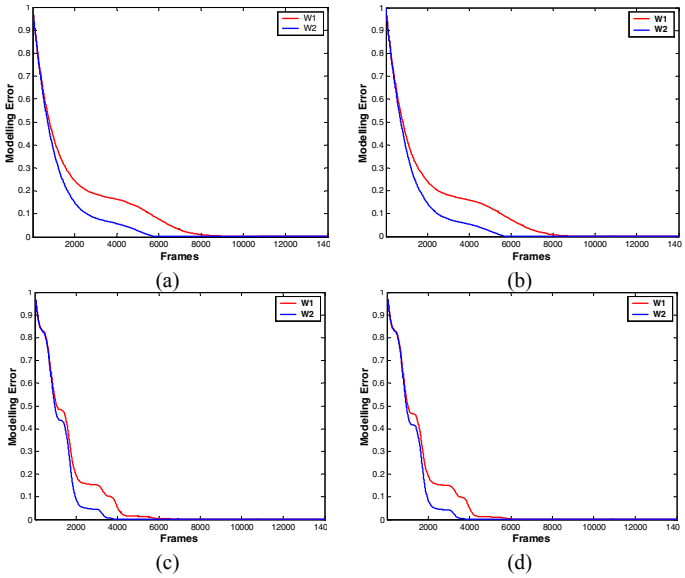

Figure 7. Modelling error for (a), (c) QPSK and (b), (d) 16-QAM case for slow and fast fading respectively.

TABLE I. RESULTS FOR SLOW AND FAST FADING RAYLEIGH MULTIPATH ENVIRONMENTS.

Modulation type		Before Correction			After Correction		
		α_ε (dB)	φ_ε°	IRR (dB)	α_ε (dB)	φ_ε°	IRR (dB)
Slow Fading	QPSK	3	30	10.0	0.0031	2.7e-4	73.1
	16-QAM				0.0030	2.4e-4	73.5
Fast Fading	QPSK				0.0030	2.7e-4	73.2
	16-QAM				0.0026	2.6e-4	74.1

D. *Different Modulation Formats and Low SNR*

The performance of the proposed algorithm under low SNR values and different modulation formats and constellation sizes is shown in Table II. The SNR required to achieve 10^{-1} BER is computed for 8-PSK and 32-PSK as well as 32-QAM and 256-QAM cases. As can be observed form Table II, the algorithm is able to eliminate the phase and gain errors. IRR in the order of 75–97 dB after DIRP was shown to be achievable. This IRR is much more than the required amount.

TABLE II. PARAMETER VALUES FOR BER OF 10^{-1}.

Modulation type	Before Correction				After Correction				
	Gain Error (dB)	Phase Error (deg)	$\|h_1\| = \|h_2\|$	IRR (dB)	Gain Error (dB)	Phase Error (deg)	$\|w_1\|$	$\|w_2\|$	IRR (dB)
8-PSK SNR= 5.6 Eb/No=0.87	3	30	0.6090	10.0	1.9e-4	3.7e-5	0.6089	0.6091	75.5
	2	15	0.3461	15.2	0.0145	5.0e-5	0.3460	0.3460	83.2
	1	7.5	0.1740	21.2	0.0073	1.7e-6	0.1740	0.1739	96.9
32-PSK SNR=13.7 Eb/No=6.7	3	30	0.6090	10.0	0.0012	2.4e-4	0.6086	0.6085	75.3
	2	15	0.3461	15.2	0.0034	8.7e-5	0.3459	0.3461	80.3
	1	7.5	0.1740	21.2	0.0218	1.9e-4	0.1740	0.1739	95.8
32-QAM SNR=15.5 Eb/No=8.5	3	30	0.6090	10.0	9.1e-4	2.4e-4	0.6086	0.6086	74.8
	2	15	0.3461	15.2	0.0120	6.8e-5	0.3459	0.3461	80.8
	1	7.5	0.1740	21.2	0.0032	7.2e-5	0.1741	0.1740	86.9
256-QAM SNR=24.9 Eb/No=15.9	3	30	0.6090	10.0	0.0068	7.1e-5	0.6084	0.6087	73.3
	2	15	0.3461	15.2	0.0108	3.9e-5	0.3459	0.3459	78.9
	1	7.5	0.1740	21.2	0.0045	4.7e-5	0.1739	0.1739	91.1

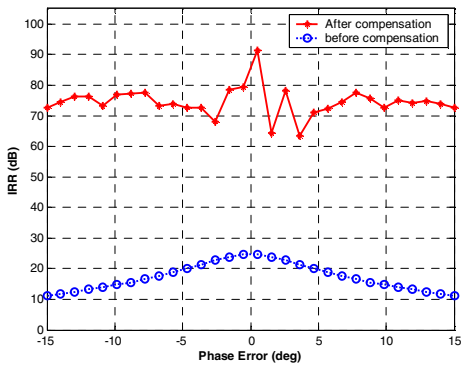

Figure 8. IRR before and after compensation for varying phase error.

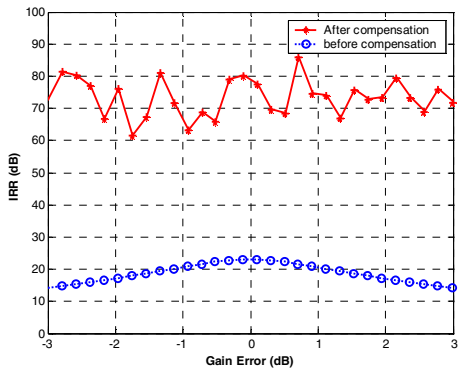

Figure 9. IRR before and after compensation for varying gain error.

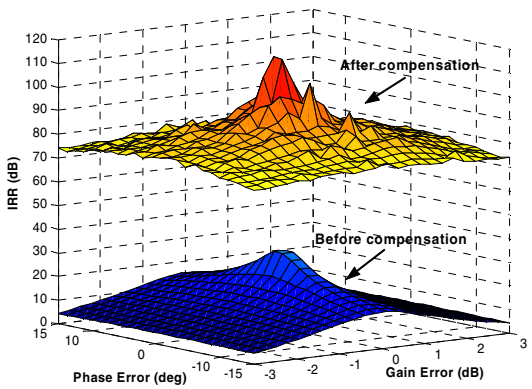

Figure 10. 3-D visualisation of IRR before and after compensation, varying both phase and gain errors.

IV. CONCLUDING REMARKS

Adaptive self-calibrating image rejection architecture capable of achieving IRR values from 75-97 dB after compensating has been described. The algorithm is very simple to implement consisting of two, single-tap-complex adaptive FIR filters with LMS coefficient update hardware.

The algorithm enables fast and very accurate I/Q imbalance compensation in the whole receiver chain at low cost. Algorithm is able to work under multipath and Rayleigh fading environments as well as under low SNR. It works on-the-fly and is able to track time-varying errors. It works with any type of modulation formats and constellation sizes. The proposed structure greatly relaxes the analog-frontend specification enabling high levels of integration and leading a path to single chip radio receiver.

Next phase of the research is to prototype this structure on FPGA and run it in real-time and compare the performance that can be achieved with the simulation results.

REFERENCES

[1] M. D. McDonald, "A 2.5GHz BiCMOS image-reject front-end," *ISSCC Dig. of Tech. Papers*, pp. 144–145, Feb. 1993.

[2] W. Baumberger, "A single-chip image rejecting receiver for the 2.44 GHz band using commercial GaAs-MESFET-technology" *IEEE Journal of Solid-State Circuits*, , vol. 29 issue. 10, pp. 1244 -1249, Oct. 1994.

[3] Pache, D.; Fournier, J.M.; Billiot, G.; Senn, P.; "An improved 3 V 2 GHz BiCMOS image reject mixer IC" *IEEE Custom Integrated Circuits Conference*, pp. 95 -98, May 1995.

[4] Maligeorgos, J.P.; Long, J.R., "A low-voltage 5.1-5.8-GHz image-reject receiver with wide dynamic range"; *IEEE Journal of Solid-State Circuits*, vol. 35, issue: 12 , pp. 1917 -1926, Dec 2000.

[5] F. Ehbahani, Y. Ishigami, J. Leete and A.A. Abidi, "CMOS mixers and polyphase filters for large image rejection" *IEEE Journal of Solid-State Circuits*, vol. 36, pp. 873 -887, June 2001.

[6] L. Der, B. Razavi, "2-GHz CMOS image-reject receiver with LMS calibration" *IEEE Journal of Solid-State Circuits*, , vol. 38 pp. 167 -175, Feb. 2003.

[7] C. C. Chen, C. C. Huang, "On the architecture and performance of a hybrid image rejection receiver", *IEEE Journal on Selected Areas in Communications*, vol. 19, pp. 1029 -1040, June 2001.

[8] Cetin, E.; Kale, I.; Morling, R.C.S., "Adaptive digital receivers for analog front-end mismatch correction", *IEEE VTS 54th Vehicular Technology Conference (VTC 2001 Fall)*, vol: 4, pp. 2519 –2522, 2001.

[9] Widrow B. and S.D. Stearns, "*Adaptive Signal Processing*", Prentice Hall, 1985, ISBN: 0-13-004029-0.